Available online at www.sciencedirect.com
ScienceDirect
Journal of the European Ceramic Society 27 (2007) 4639–4647
www.elsevier.com/locate/jeurceramsoc

Development of celsian ceramics from fly ash useful for X-ray radiation-shielding application

S.S. Amritphale *, Avneesh Anshul, Navin Chandra, N. Ramakrishnan

Regional Research Laboratory, Habib Ganj Naka, Hoshangabad Road, Bhopal 462026, Madhya Pradesh, India

Received 16 November 2006; received in revised form 7 March 2007; accepted 16 March 2007
Available online 13 June 2007

Abstract

For the first time the capability of fly ash to produce barium containing radiopaque materials has been demonstrated. Fly ash which is a waste generated in power plants due to combustion of pulverized coal, has been utilized[a] for making X-ray radiation-shielding materials. A novel method for making radiation-shielding materials utilizing fly ash and barium compound has been developed by ceramic processing route using phosphate bonding. The fly ash based radiopaque materials (FARM), i.e. shielding materials are characterized for their X-ray attenuation characteristics. The shielding, i.e. half value thickness (HVT) for different energies of X-ray photons for FARM have been computed and compared with conventionally used shielding materials, namely concrete and lead, it is found that the HVT of the fly ash based shielding materials, in comparison to concrete, is significantly very less for the various energies of X-ray photons.

The X-ray powder diffraction studies confirmed the presence of monoclinic and hexagonal celsian and sanbornite as the major shielding phases and potassium aluminosilicate, sodium aluminosilicate and silicophosphate as the binder phases in the FARM and are responsible for providing bonding to the ceramic matrix leading to the effective shielding and mechanical properties. Scanning electron microphotographs have revealed the compacted plate like particles with hexagonal morphological characteristics of the various barium silicate and barium aluminosilicate (BAS) shielding phases in the matrix of radiopaque materials. The mechanical properties, namely compressive strength and impact strength evaluation test showed that FARM meets the standard specifications laid down for radiation-shielding concrete and ceramic tiles. Based on the above studies, it is found that FARM, can preferably be used for the construction of X-ray diagnostic and CT-scanner room to provide adequate shielding against X-ray photons.

Keyword: Fly ash

1. Introduction

The celsian, i.e. barium aluminosilicate (BAS) is well known for its applications in refractories, porcelains, glass ceramics and electrical insulators.[1,2] Recently, the application spectrum of BAS has further extended for potential application: (a) as a ceramic matrix for high temperature composites[3,4] and (b) in making cast prostheses for biomedical application because of their radiopacity and better strength in comparison to conventional feldspathic porcelains and ease of imparting desired shape by adopting glass ceramic processing route of fabrication.[5] Silica glasses containing barium, e.g. SiO_2–Al_2O_3–BaO have been used as radiopaque filler for dental composites. Radiopacity in these materials results from the incorporation of an element of relatively high atomic numbers such as barium and strontium into the ceramic matrixes such as silica and aluminium silicate structure, i.e. sanbornite and celsian.[6] Further studies on the: (i) effect of barium addition[7] on the densification and mullitization of silica and alumina raw materials is found to increase densification and greater glassy phase formation and thus leading to high mechanical strength of the ceramic materials and (ii) increase in the barium content increases the radiopacity of the materials.[8] There is growing interest of developing alternate barium aluminosilicate phosphate glass ceramics for immobilization[9] of radioactive waste due to their radiopacity and ability to host variety of radioactive element in their glassy matrix.

The synthesis of celsian can be carried out by using a variety of raw materials and processing methods ranging from

* Corresponding author. Tel.: +91 755 2587244; fax: +91 755 2587042.
E-mail address: ssamritphalerrl@yahoo.co.in (S.S. Amritphale).

[a] Patent applications for the developed process have already been flied in USA as well as in India vide Application No. US PTO-2646690000/03/30/06 #20060066013 and 1888/Del/04, respectively.

0955-2219/$ – see front matter © 2007 Elsevier Ltd. All rights reserved.
doi:10.1016/j.jeurceramsoc.2007.03.034

traditional glass ceramics[10] calcinations of natural and synthetic solid salt/oxide mixtures,[11,12] (e.g. kaolin, topaz, alumina, silica, barium sulphate, barium carbonate), solid metal oxidation,[1,2] e.g. barium, aluminium, alumina, silica to sol–gel,[13–15] e.g. barium aluminosilicate gel, barium exchanged zeolite, etc. These various processing routes involves homogenization of appropriate ratios of raw materials and heat treatment in the presence of air in the temperature range of 900–1530 °C for a duration of 4–40 h. Further, many researchers have studied the enhancement of the formation kinetics of intermediate compound during the formation of celsian using different raw materials mixtures and it is reported that by using starting materials possessing aluminium silicate structure helps in lowering the hexacelsian formation temperature significantly.[3] Since fly ash contains (Veloza et al., www.japws.jp/proceeding/symposium 05/360 Matamoros) aluminium silicate structures, e.g. mullite and highly reactive amorphous aluminosilicate vitreous as major mineralogical phases apart from the quartz, the fly ash can be used as a potential resource starting materials for making barium containing radiopaque celsian glass ceramics,[8] refractory cements such as, barium silicate, barium aluminate.[17,18] It is reported that barium aluminate is being used as an indispensable component in the Portland cement mixture and as a fundamental materials in the construction of nuclear reactors.[19] Recently, an environmental barrier multi-layer coating has also been developed based on a composition containing celsian, i.e. barium aluminosilicates and mullite[20] as the presence of mullite in the mullite/celsian glass ceramics increases the high temperature strength.[21] The use of fly ash for the preparation of mullite[22] and cordierite[23] is also reported in the literature. Fly ash is often used as a low cost source of aluminosilicate in ceramic industries, because it contains appropriate content of silica and alumina in the form of mullite, quartz and siliicoaluminous phases.[24] It is reported[25–27] that the mineralogical composition of typical class of fly ash shows the presence of non-magnetic phases, namely mullite ($Al_6Si_2O_{13}$) 25–30 wt%, α quartz (α-SiO_2) 9–12 wt%, silicoaluminous glassy phase 62 wt% and magnetic phases, namely magnetite (Fe_3O_4) 4–6 wt%, hematite (Fe_2O_3) 1–3 wt%, etc. The glassy character of fly ash makes it a potential candidate as solid precursor for developing glass ceramic materials.[28] Million tonnes of fly ash are generated in coal based thermal power plants all over the world. In India alone more than 90 million tonnes of fly ash is produced annually which requires more than 65,000 acres of land being used for its dumping.[29]

From the foregoing discussion it is clear that the fly ash possess unique aluminosilicate mineralogical compositions, i.e. mullite, aluminosilicate glassy phase and quartz which facilitates the formation of radiopaque celsian ceramics. In view of above, studies on development of celsian based radiopaque materials by sintering fly ash with barium compounds has been carried out. The characterization of fly ash based celsian ceramics for: (i) X-ray attenuation characteristics and (ii) mechanical properties, namely compressive and impact strength has shown that these materials can be used for the construction of X-ray diagnostic and CT-scanner room. The results of these studies are presented in this paper.

2. Materials and methods

2.1. Raw materials and chemicals

The fly ash from Thermal Power Plant, Sarni district Betul (M.P.), India, has been collected and was used as received, after making a representative sample by the method of coining and quartering. The barium hydroxide and sodium hexameta phosphate, chemicals of GR grade of Merck make India, were used as such without any further purification.

2.2. Preparation of green tile samples and their sintering

The samples of shielding materials in the form of ceramic tiles and cubes were prepared based on our earlier research investigation on sintering characteristics of red mud, fly ash and pyrophyllite.[30–34] The raw material mixtures were prepared by homogenizing fly ash with barium hydroxide additions up to 50 wt% at 10% increments. The mixtures obtained were homogenized with 10 wt% sodium hexameta phosphate binder aqueous solutions (Table 1). After homogenization, the raw mix was then compressed in a steel mould at a pressure of 300 kg/cm^2 (using, Digital compression testing machine, model no. AIM 308E-DG of AIMIL Ltd. India make), to obtain samples of tiles of dimension 10 cm × 10 cm × 2.0 cm and samples of cube of dimension 5 cm × 5 cm. The green samples were then dried in an air oven at 110 °C for 1-h duration and then sintered in an electrical muffle furnace. The firing cycle was programmed as follows: heating from ambient temperature to 100, 200, 300 and 400 °C at a heating rate of 10 °C/min, holding for 30 min at 400 °C; heating to 1100 °C at rate of 10 °C, holding for 60 min at 1100 °C; and finally cooling of samples in the furnace itself down to ambient temperature.

2.3. Determination of X-ray attenuation characteristics

The determination of X-ray attenuation characteristics of shielding material was carried out in the Standard Safety System Division of Bhabha Atomic Research Center (BARC), Mumbai, India, under following measurement conditions:

(i) Measurements were done with (I) and without filters (I_o) to determine the tenth value thickness (TVT) of the beams.
(ii) Measurements were done at a distance of 60 cm from the surface of the cone to the center of the chamber (i.e. at a distance of 100 cm from the X-ray focal spot).
(iii) Dose rate meter UNFORS Instrument (Sweden) type 9001, sr. no. 12394.
(iv) Measurements were done in charge mode and leakages were noted and corrected.
(v) Temperature and pressure were measured using calibrated thermometer and barometer and the readings were corrected for the same. The measurement uncertainty may be ± within 5%. For evaluating X-ray attenuation characteristics the shielding materials samples were made in the form of cir-

Table 1
Raw materials proportions used for making various compositions of shielding materials

Sr. No.	Composition code	Quantity of fly ash (%)	Quantity of barium hydroxide (%)	Quantity of sodium hexameta phosphate (%)
1.	F1	80	10	10
2.	F2	70	20	10
3.	F3	60	30	10
4.	F4	50	40	10
5.	F5	40	50	10

cular disc of 25 mm diameter and 9, 10, 12, and 17 mm thickness.

2.3.1. Determination of the mechanical properties of the shielding materials

The bulk density determination has been performed as per the standard procedure prescribed for ceramics.[35] The sintered tiles samples of size 10 cm × 10 cm × 2.0 cm were evaluated for their impact strength following the procedure laid down in the specifications drawn for ceramic tiles.[36]

The procedure for measuring impact strength involved use of failing weight type instrument. The impact strength was carried out by placing the bottom surface of the tile on a 60 mm equilateral triangular support. A steel ball of 30 g weight was allowed to drop on the top surface of the tile sample from an initial height of 25 cm. The height of the free fall of the steel ball was increased in small increments till failure. Impact strength was calculated as per the formula.

$$\text{Impact strength} = \frac{W \times h}{t},$$

where W is the weight of the steel ball (kg), h the height of free fall of steel ball (m), and t is the thickness of the tile (cm).

The compressive strength measurement of the cube of shielding material was performed as per the standard procedure prescribed for the testing of concrete.[36] The measurement were carried out using Digital compressive strength testing machine, model no. AIM 308E-DG of AIMIL Ltd. India make. The dimension of the shielding samples for compressive strength evaluation was of 5 cm × 5 cm size and kept constant for all the composition studied.

2.3.2. Investigation of phases formed in the sintered shielding materials

The investigation of various phases formed in the sintered shielding materials made using optimized processing parameters was carried out using a Philips model 1710 X-ray diffractometer, using Ni filtered Cu Kα radiation.

2.3.3. Morphology of powdered sintered shielding material sample

The morphology of the various phases formed in the shielding tile samples made using optimized processing parameters was studied using a JEOL model JEM-35-CF scanning electron microscope.

3. Results and discussion

3.1. Characterization of fly ash

The chemical composition of fly ash was determined by standard wet chemical analysis method of chemical analysis.[37] The chemical analysis showed (cf. Fig. 1) that the various oxide percent content (wt%) as follows: SiO_2, 62.12; Al_2O_3, 21.30; Fe_2O_3, 5.55; TiO_2, 1.38; MgO, 1.58; CaO, 0.53; K_2O, 4.24%, respectively. The loss on ignition was found to be 3.30%. The wet sieve analysis of fly ash shows that the 78% of the particles are below 48 μm size.

3.2. Phases identification in sintered shielding materials

Identification of the various phases present in the fly ash as such (F) and formed during sintering in the different shielding material compositions F1–F5 was carried out by comparing the experimental inter planar spacing (d values) with those of the respective likely substances listed in the JCPDS[38] standard X-ray diffraction data files. The XRD patterns obtained are given in Figs. 2–7.

The results of chemical analysis and X-ray powder diffraction analysis of fly ash exhibited the presence of a diverse mineralogical phases and compounds which act as a source materials for obtaining varieties of shielding phases (cf. Fig. 2). The XRD of fly ash (F) shows the presence of mullite ($Al_6Si_2O_{13}$), quartz, and silicoaluminous glassy phase as the major phases and hematite as accessory phase. The vitreous aluminosilicate glassy and mullite phases present in the fly ash facilitate the formation of barium aluminosilicate, i.e. celsian, and the content of quartz help in obtaining sanbornite, i.e. barium silicate and silicophosphate phases, respectively. The use of phosphatic

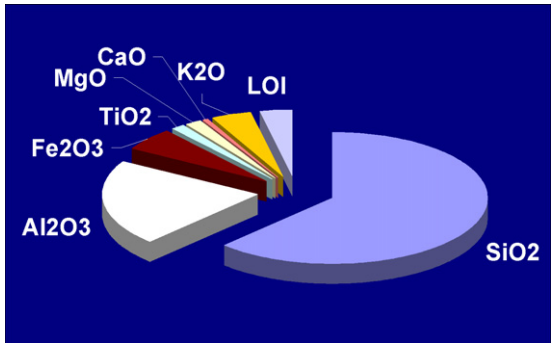

Fig. 1. Chemical analysis of fly ash and major prospective shielding constituents.

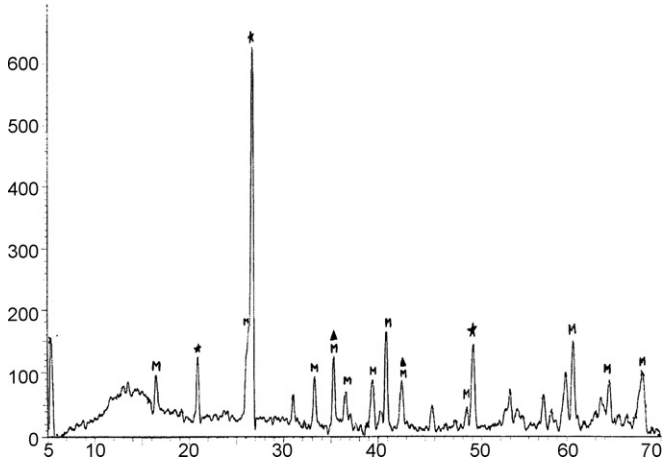

Fig. 2. XRD of fly ash (*) quartz, (M) Mullite, (▲) hematite.

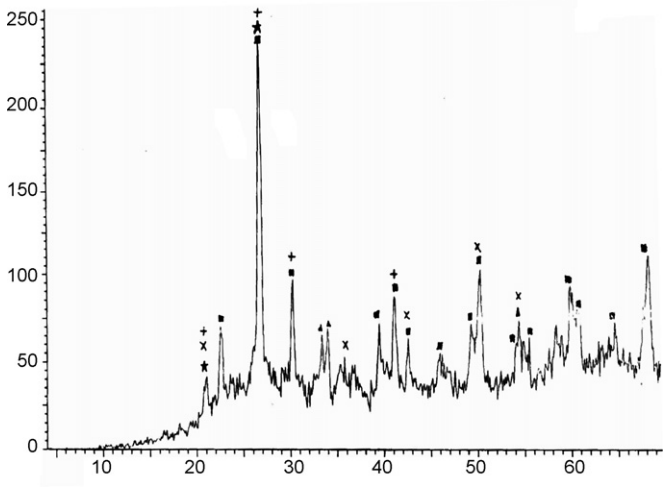

Fig. 3. XRD of F1: (*) quartz, (▲) hematite, (+) potassium aluminium silicate, (■) celsian $BaAl_2Si_2O_8$.

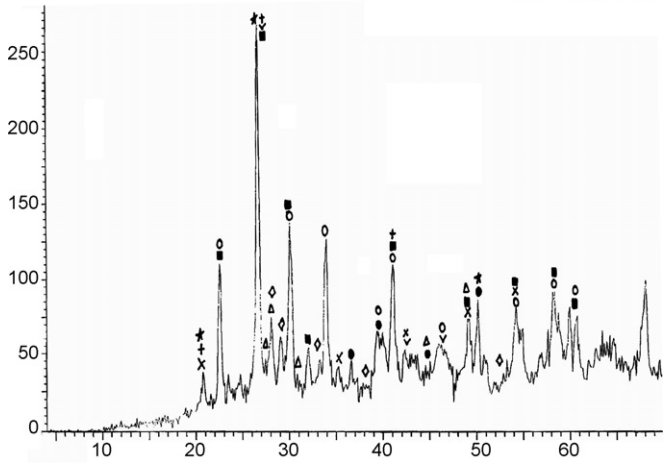

Fig. 4. XRD of F2: (*) quartz, (■) celsian $BaAl_2Si_2O_8$, (+) potassium aluminium silicate, (×) sodium aluminium silicate, (√) silicophosphate, (◊) barium silicate $BaSi_2O_5$, (△) barium aluminate, (◯) $BaAl_2Si_2O_8$.

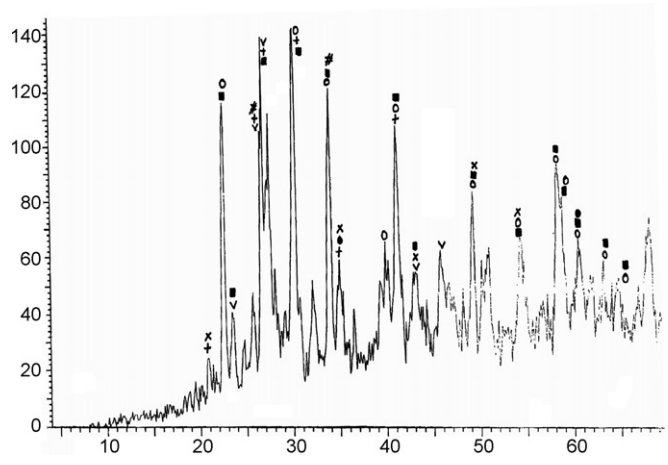

Fig. 5. XRD of F3: (◯) $BaAl_2Si_2O_8$, (+) potassium aluminium silicate, (×) sodium aluminium silicate, (■) celsian $BaAl_2Si_2O_8$, (√) silicophosphate, (#) $BaFe_2O_4$.

binders such as sodium hexa metaphosphate has been found to be effective in lowering sintering temperature[34] and leads to the formation of crystalline silicophosphate. The potassium and iron oxide content of fly ash forms the potassium aluminosilicate and barium ferrite phases, respectively.

The XRD of composition (cf. Fig. 3) F1 shows the formation of new phases of monoclinic celsian, sodium aluminosilicate and potassium aluminosilicate, respectively. In the celsian formation system, generally it is reported that the formation of hexacelsian takes place first and during the heat treatment it gets converted to celsian, but in the present studies of making celsian using fly ash we noted that celsian has formed first and not the hexacelsian; similar observations are reported in literature.[39,40]

The intensity of quartz peak reduces and the peak observed for mullite in the fly ash (F) sample is found to disappear completely. These observations are attributed to the formation of celsian at the expense of mullite[39] and quartz. Similar observations have been reported[17] during the formation of dibarium silicate refractory cement at the expense of mullite.

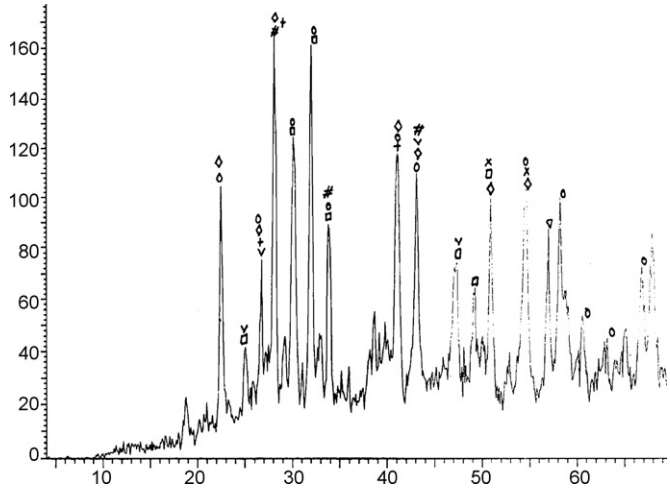

Fig. 6. XRD of F4: (◊) barium silicate $BaSi_2O_5$, (+) potassium aluminium silicate, (×) sodium aluminium silicate, (√) silicophosphate, (#) $BaFe_2O_4$, (△) barium aluminate, (◯) $BaAl_2Si_2O_8$.

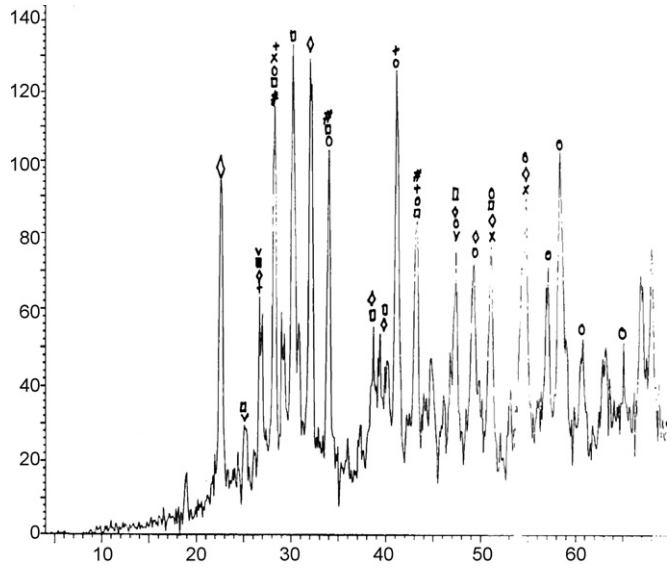

Fig. 7. XRD of F5: (◯) $BaAl_2Si_2O_8$, (+) potassium aluminium silicate, (×) sodium aluminium silicate, (■) celsian $BaAl_2Si_2O_8$, (√) silicophosphate, (#) $BaFe_2O_4$, (◊) barium silicate $BaSi_2O_5$.

The XRD of composition F2 (cf. Fig. 4) shows the formation of new phases of barium silicate (sanbornite), barium aluminate, hexagonal celsian, silicophosphate and magnetite. The barium hydroxide reacts with silica and alumina content of the fly ash and leads to the simultaneous formation of barium silicate and barium aluminates.[41] The intensity of quartz peak further reduces whereas the intensity of monoclinic celsian, sodium aluminosilicate and potassium aluminosilicate increases further. The XRD of composition F3 (cf. Fig. 5) shows the presence of a new peak of barium ferrite and disappearance of peak due to magnetite, barium silicate (sanbornite) and barium aluminate. These observations are ascribed to: (i) the formation of barium ferrite by the reaction of magnetite and barium compounds, (ii) the formation of increased content of monoclinic and hexagonal celsian by the reaction of barium silicate (sanbornite) and barium aluminate with alumina and silica content of fly ash, respectively.[42] This fact is further confirmed as the intensity of monoclinic and hexagonal celsian, sodium aluminosilicate and potassium aluminosilicate is found to increase further.

The XRD of composition F4 (cf. Fig. 6) shows the presence of a new peak of silica deficient hexagonal celsian and reappearance of sanbornite phase. The XRD of composition F5 (cf. Fig. 7) shows the further increase in the intensity of hexagonal celsian, sodium aluminosilicate and potassium aluminosilicate and silicophosphate phases.

3.3. Morphology of powdered sintered shielding material compositions

The scanning electron micrographs exhibiting microstructure of fly ash as such (F) and of different shielding compositions, namely F1–F5 are given in Figs. 8–13, respectively. The formation of sodium aluminosilicate, potassium aluminosilicate and silicophosphate promotes liquid phase sintering in the fly ash based ceramics leading to the formation of very dense matrix

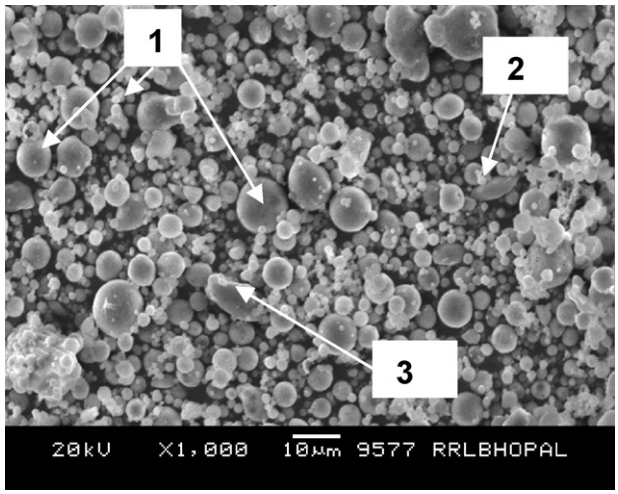

Fig. 8. SEM of fly ash composition: (1) sphere/cenospheres, (2) elongated needle mullite, (3) euhedral quartz.

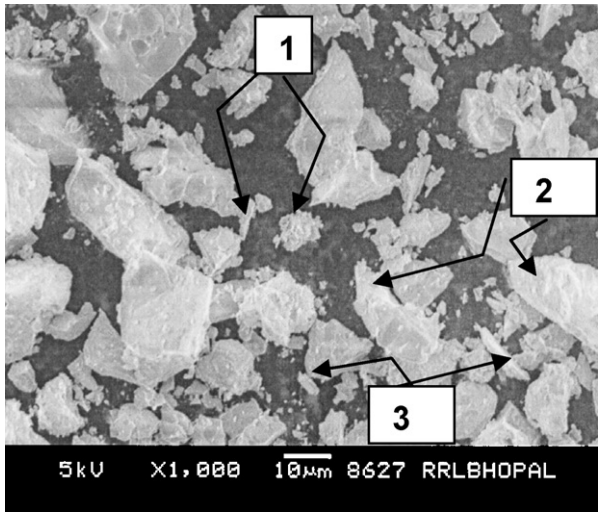

Fig. 9. SEM of F1 composition: (1) spherical hematite, (2) euhedral quartz, (3) monoclinic celsian $BaAl_2Si_2O_8$.

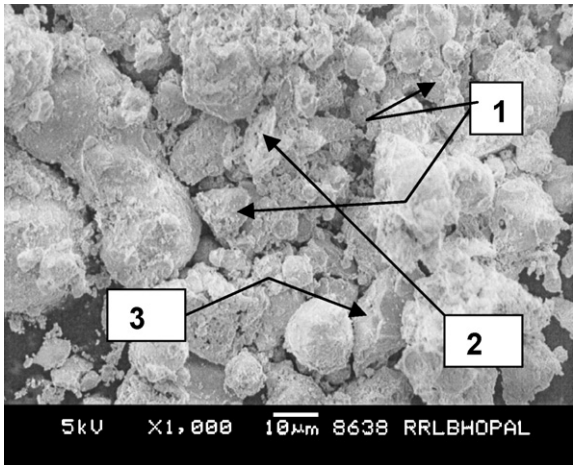

Fig. 10. SEM of F2 composition: (1) monoclinic celsian, (2) hexagonal celsian, (3) euhedral quartz.

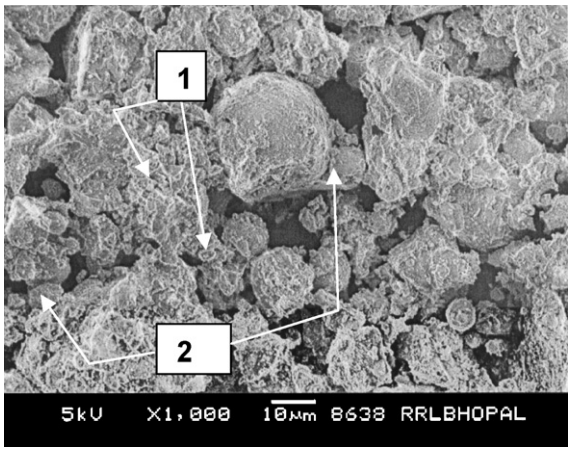

Fig. 11. SEM of F3 composition: (1) monoclinic celsian, (2) hexagonal celsian.

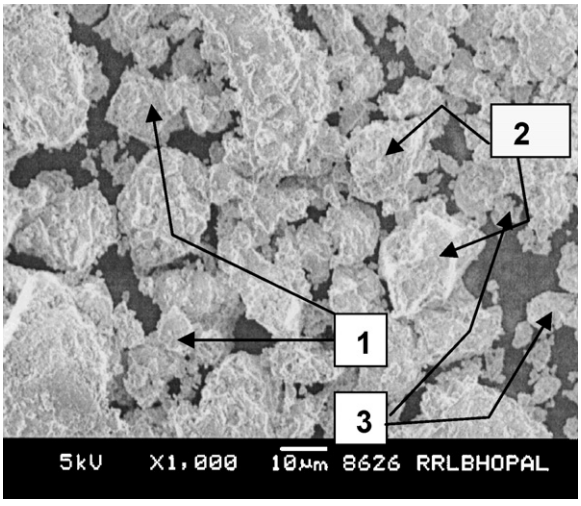

Fig. 12. SEM of F4 composition: (1) monoclinic celsian, (2) hexagonal celsian, (3) barium silicate.

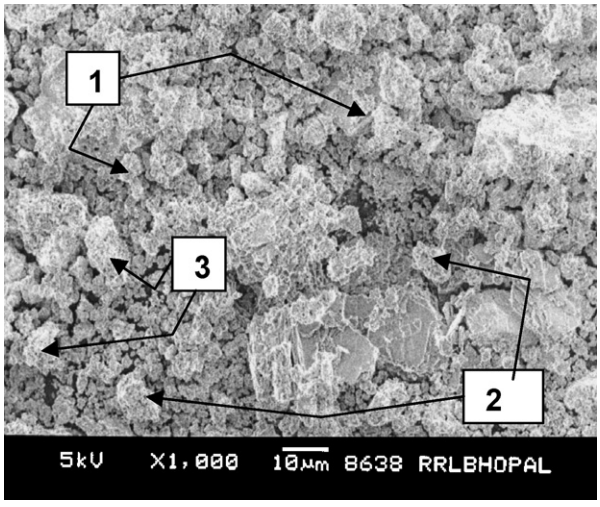

Fig. 13. SEM of F5 composition: (1) monoclinic celsian, (2) hexagonal celsian, (3) barium silicate.

which is responsible for providing high mechanical strength and effective shielding. The micrographs of shielding sample clearly show the compacted and continued integrated morphological characteristics. The micrograph[16,43] of fly ash clearly reveals (cf. Fig. 8) the typical vitreous amorphous aluminosilicate glassy phase agglomerate of sphere or cenospheres, which is more reactive than the crystalline mullite having elongated needle characteristics and quartz having euhedral and subhedral characteristics.

The SEM micrograph of composition F1 (cf. Fig. 9) shows the monoclinic plate like morphology[44,45] celsian and hexagonal and rhombohederal morphology of sodium aluminium silicate and potassium aluminium silicate, respectively.

The SEM micrograph of composition F2 (cf. Fig. 10) shows the additional morphology[46] of orthorhombic and euhedral crystals of barium silicate[17] and spherical[34] particles of silicophosphates.

The SEM micrograph of composition F3 (cf. Fig. 11) shows[46] the excessive formation of dense surface texture of compacted monoclinic and hexagonal-barium aluminium silicates in addition to few crystals of barium ferrite. The SEM of composition F4 (cf. Fig. 12) shows the reappearance of orthorhombic and euhedral and subhedral crystals of barium silicate in addition to monoclinic and hexagonal-barium aluminium silicates.[17]

Similarly, the SEM of composition F5 (cf. Fig. 13) exhibits the still more concentrated and compacted texture of phases as revealed in the composition F4.

3.4. Determination of the attenuation characteristics of the shielding materials

With a view to find applicability of shielding materials in the area of: (a) diagnostic X-ray and (b) CT-scanner facilities the materials have accordingly been evaluated at 100, 150, 200 and 250 kV effective energies of X-ray photon. The results of narrow beam X-ray attenuation characteristics of shielding materials at various effective energy of X-ray photons in terms of: (i) percentage shielding for different compositions are shown in Fig. 14 and (ii) the half value thickness (HVT) are given in Figs. 15–18. The effect of barium content in the various compositions clearly shows that the percentage shielding increases with increase in barium content from F1 to F5. Taira et al.[8] have reported similar observations.

On the basis of attenuation data obtained for different compositions, the half value thickness has been computed and

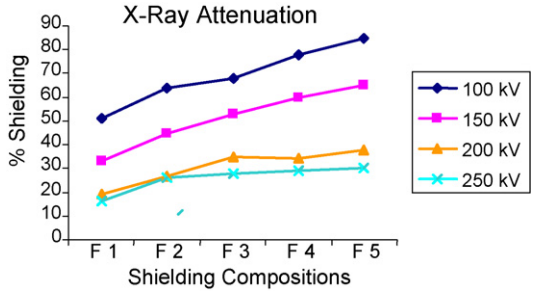

Fig. 14. Percentage shielding of different compositions.

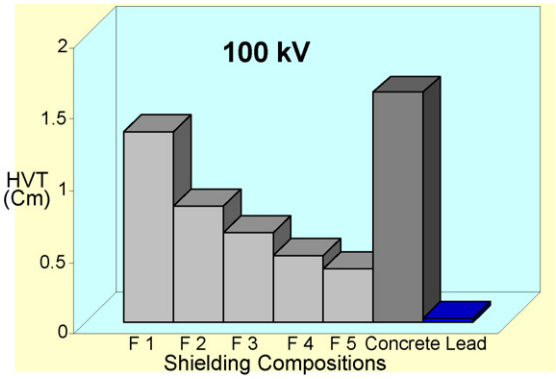

Fig. 15. Attenuation at 100 kV X-ray.

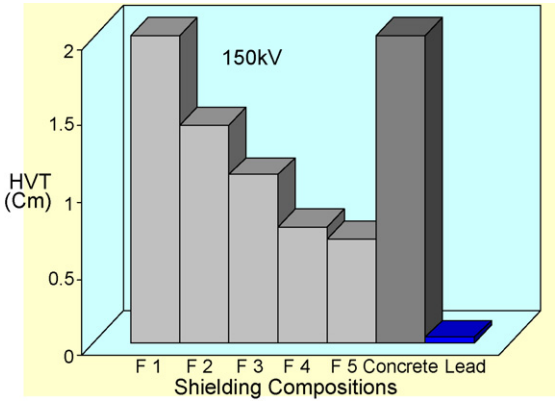

Fig. 16. Attenuation at 150 kV X-ray.

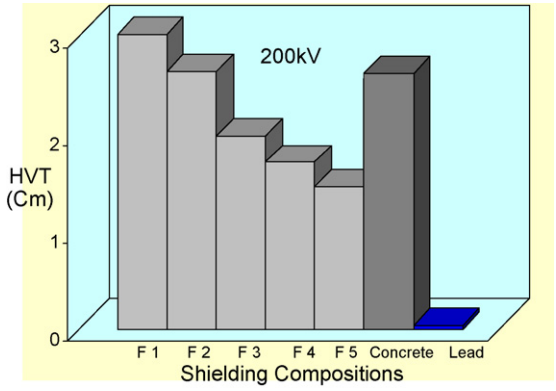

Fig. 17. Attenuation at 200 kV X-ray.

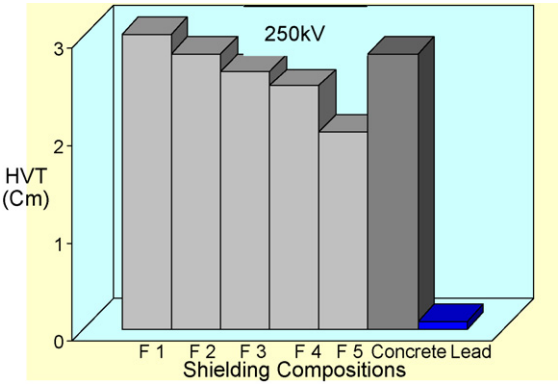

Fig. 18. Attenuation at 250 kV X-ray.

Table 2
Comparison of shielding thickness in terms of half value thickness (HVT) of fly ash based shielding compositions with lead and concrete, for different energies of X-ray photons

kVp of X-ray beam	Lead	Concrete	F1	F2	F3	F4	F5
100	0.025	1.6	1.33	0.8107	0.6215	0.4601	0.3647
150	0.029	2.2	2.1983	1.4161	1.0943	0.7579	0.6762
200	0.042	2.6	4.106	2.625	1.963	1.698	1.452
250	0.080	2.8	4.593	2.7964	2.6168	2.4748	2.0048

Shielding thickness, i.e. HVT (cm).

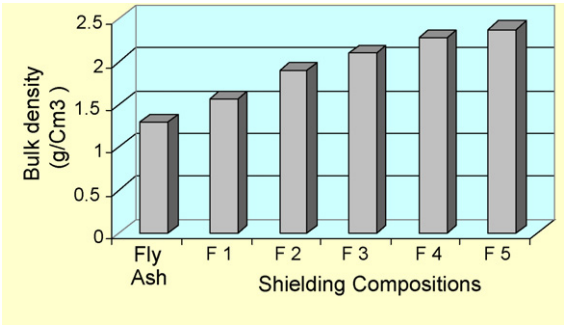

Fig. 19. Density of fly ash based shielding compositions.

compared[47] with conventional concrete and lead materials. From the HVT values of shielding materials at various energies of X-ray photons, it is found that shielding materials can preferably be used for the construction of X-ray diagnostic and CT-scanner room to provide adequate shielding against X-ray photons (Table 2).

3.5. Mechanical properties of shielding materials

The result of bulk density determination of various compositions of shielding material is given in Fig. 19. The result shows

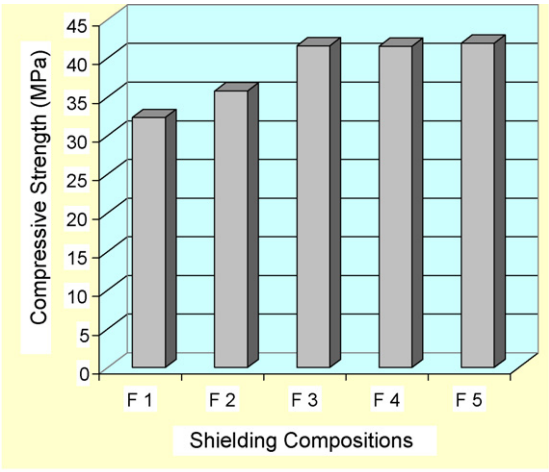

Fig. 20. Compressive strength of shielding compositions.

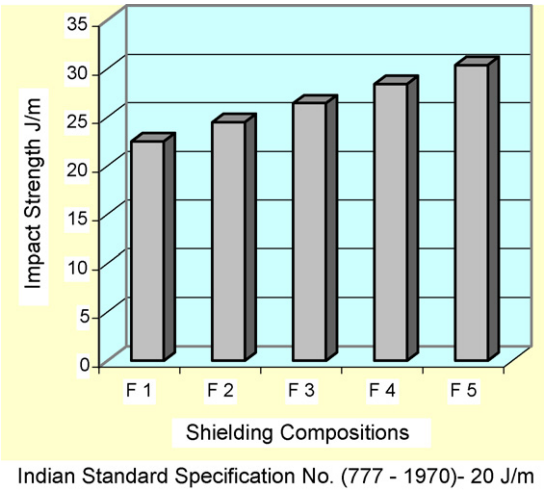

Fig. 21. Impact strength of shielding compositions.

that bulk density increases with the increase of barium content in the shielding compositions.

Shielding materials of F5 composition possesses significant high bulk density, i.e. up to 2.38 g/cm^3 in comparison to 1.34 g/cm^3 of fly ash.[30,31] This increased bulk density is responsible for imparting effective shielding to the developed fly ash based radiopaque materials (FARM).

For evaluating the compressive and impact strength of the shielding materials, samples were made in the form of cube and ceramic tiles, respectively. The results obtained for compressive strength and impact strength determination are given in Figs. 20 and 21, and it is found that shielding materials samples made from composition F1 to F5 meets the requirement of compressive and impact strength prescribed in the Indian standard specification no. 9103-1999, and no. 777-1970 for ceramic tiles and concrete, respectively. Therefore, shielding materials can be used as structural materials for the X-ray diagnostic and CT-scanner room installation.

4. Conclusions

The capability of fly ash to produce barium containing radiopaque materials has been demonstrated. The presence of aluminosilicate structure, i.e. mullite and highly reactive amorphous aluminosilicate glassy phase, and quartz in the fly ash highly facilitates the formation of various barium containing shielding phases, namely monoclinic and hexagonal celsian, sanbornite and barium aluminates, etc. The results obtained represent a fundamental starting point for utilization of fly ash in mixture with barium compounds, as resource material for making barium containing silicates and aluminosilicates, useful for X-ray shielding applications.

The shielding thickness (HVT) of the fly ash based shielding composition (F5), in comparison to concrete, is significantly very less for the various energies of X-ray photons, i.e. 100, 150, 200 and 250 kV and therefore fly ash based shielding materials can provide effective shielding at very less thickness itself. The fly ash based radiopaque materials conform to the requirement of compressive strength and impact strength as specified by standards for shielding concrete and ceramic tiles. The FARM have exhibited the most effective shielding for 100 kV X-ray and adequate strength requirement of structural materials and therefore can preferably be used for the construction of X-ray diagnostic and CT-scanner room.

The XRD studies of the FARM sample have confirmed the presence of different shielding phases, namely monoclinic and hexagonal-barium aluminium silicate, celsian and sanbornite as the major shielding phases and potassium aluminosilicate, sodium aluminosilicate and silicophosphate as the binder phases in the FARM and are responsible for providing bonding to the ceramic matrix leading to the effective shielding and mechanical properties. The SEM of the shielding compositions have clearly revealed the compacted plate like particles of monoclinic and hexagonal characteristics of the various shielding phases in the fly ash based barium aluminosilicate system.

The studies have opened up the possibility of developing fly ash based radiopaque cementious materials, namely barium silicates and barium aluminate, barium aluminosilicates useful for refractory and as admixture in Portland cement mix of nuclear reactors, respectively.

Acknowledgements

The authors are thankful to the Board of Research in Nuclear Science, Mumbai, India, for sponsoring (2004/36/26-BRNS/1936) the research work on development of shielding materials utilizing fly ash. Special thanks are due to Shri. V.S. Patki, Shri. V.V. Shaha and Shri. Bhutani of Bhabha Atomic Research Centre, Mumbai, and Shri Arvind Shrivastava, Nuclear Power Corporation India Limited, India, for their kind help in arranging X-ray attenuation test of the shielding materials and fruitful discussion.

References

1. Zhang, X.-D., Sandhage, K. H. and Fraser, H. J., Synthesis of $BaAl_2Si_2O_8$ from solid Ba–Al–Al_2O_3–SiO_2 precursors. II: TEM analyses of phase evolution. *J. Am. Ceram. Soc.*, 1998, **81**(11), 2983–2997.
2. Allameh, S. M. and Sandhage, K. H., Synthesis of celsian ($BaAl_2Si_2O_8$) from solid Ba–Al–Al_2O_3–SiO_2precursors. I: XRD and SEM/EDX analyses of phase evolution. *J. Am. Ceram. Soc.*, 1997, **80**(12), 3109–3126.
3. Lee, K. T. and Aswath, P. B., Enhanced production of celsian barium aluminosilicates by a three-step firing technique. *Mater. Chem. Phys.*, 2001, **71**, 47–52.
4. Zhou, W., Zhang, L. and Yang, J., Preparation and properties of barium aluminosilicate glass-ceramics. *J. Mater. Sci.*, 1997, **32**, 4833–4836.
5. Griggs, J. A., Anusavice, K. J. and Mecholsky Jr., J. J., Diversification and microstructuarl coarsening of a fluoride-containing barium aluminosilicate glass. *J. Mater. Sci.*, 2002, **37**, 2017–2020.
6. Ghosh, N. N. and Pramanik, P., Synthesis of SiO_2–BaO powder by aqueous sol–gel processing for use in dental composite resins. *Br. Ceram. Trans.*, 1996, **95**(6), 267–270.
7. Quaranta, N. E. and Benavidez, E. R., Aluminosilicates compacts by alkoxide route: influence of Ba addition. *Ceramica*, 1999, **45**(2–8), 291.
8. Taira, M., Toyooka, H. and Yamaki, M., Preparation of radiopaque SiO_2–BaO fillers by the sol–gel process for dental composite resins. *Br. Ceram. Trans.*, 1994, **93**(1), 21–24.

9. Donald, I. W., Metcalfe, B. L. and Taylor, R. N. J., The immobilization of high level radioactive wastes using ceramics and glasses. *J. Mater. Sci.*, 1997, **32**, 5851–5887.
10. Bansal, N. P., Drummond, C. H. and Bahat, D., Kinetic study on the hexacelsian–celsian phase transformation. *J. Mater. Sci.*, 1970, **5**, 805.
11. Guillem Villar, M. C., Guillem Monzonis, C. and Navarro, J. A., Reactions between kaolin and barium carbonate: influence of mineralizers. 1. Qualitative study. *Trans. J. Br. Ceram. Soc.*, 1983, **82**(2), 69–72.
12. Moya Corral, J. S. and Verduchi, A. G., The solid solution of silica in celsian. *Trans. J. Br. Ceram. Soc.*, 1978, **77**(2), 40–44.
13. Chen, M., Lee, W. E. and James, P. F., Preparation and characterization of alkoxide derived celsian glass ceramics. *J. Non-Cryst. Solids*, 1990, **130**, 322–325.
14. Chen, M., Lee, W. E. and James, P. F., Synthesis of monoclinic glass ceramics from alkoxide. *J. Non-Cryst. Solids*, 1992, **147/148**, 532–536.
15. Liu, C., Komarneni, S. and Roy, R., Crystallization and seeding effect in $BaAl_2Si_2O_8$ gels. *J. Am. Ceram. Soc.*, 1995, **78**(9), 2521–2526.
16. Veloza, Z. M., Rendonangeles, J. C., Yanagisawa, K. and Cisneros-Guerrero, M. M., Densification of fly ash under alkaline hydrothermal hot pressing conditions. In *14th International Conference on the Properties of Water and Steam in Kyoto*. www.iapws.jp/Proceedings/Symposium 05/360 Matamoros-Veloza.pdf.
17. Khalil, N. M. and Zawrah, M. F., Self-formed mullite containing refractory barium silicate cements and their castable applications. *Br. Ceram. Trans.*, 2004, **103**(5), 223.
18. Zawrah, M. F. M. and Khalil, N. M., Preparation and characterization of barium containing refractory materials. *Ceram. Int.*, 2001, **27**(3), 309–314.
19. Zaki, M. I., Hussien, G. A. M. and Fahim, R. B., Characterization of the powder mixture of the reaction between alumina and barium carbonate. *J. Mater. Sci. Lett.*, 1985, **4**, 517–522.
20. Eaton, H. E. and Lawton, T. H., Method for applying a barrier layer to silicon based substrate. United States Patent (6,365,288).
21. Zhou, W., Zhang, L. and Yang, J., Preparation and properties of barium aluminosilicate glass ceramics. *J. Mater. Sci.*, 1997, **32**, 4833–4836.
22. Huang, X., Hwang, J. Y. and Mutsuddy, B. C., Properties of mullite synthesized from fly ash and alumina mixture. *Interceram*, 1995, **44**(2), 69.
23. Kumar, S., Singh, K. K. and Ramachandra Rao, P., Synthesis of cordierite from fly ash and its refractory properties. *J. Mater. Sci. Lett.*, 2000, **19**, 1263–1265.
24. Kumar, S., Das, S. K., Das, S. K. and Daspoddar, P. K., Synthesis of mullite aggregates from fly ash: effect of thermomechanical behaviour of low cement castables. *Br. Ceram. Trans.*, 2004, **103**(4), 176–180.
25. Gomes, S. and François, M., Characterization of mullite in silicoaluminous fly ash by XRD, TEM, and SiMAS, NMR. *Cem. Concr. Res.*, 2000, **30**(2), 175.
26. Matjie, R. H., Bunt, J. R. and van Heerden, J. H. P., Extraction of alumina from coal fly ash generated from a selected low rank bituminous South African coal. *Miner. Eng.*, 2005, **18**(3), 299–310.
27. Steveson, M. and Sagoecrentsil, K., Relation between composition, structure and strength of inorganic polymers. Part 2: Fly ash derived inorganic polymers. *J. Mater. Sci.*, 2005, **40**, 4247–4259.
28. Barbieri, L., Lancellotti, I., Manfredini, T., Pellacani, G. C., Rincon, J. Ma. and Romero, M., Nucleation and crystallization of new glasses from fly ash originating from thermal power plants. *J. Am. Ceram. Soc.*, 2001, **84**(8), 1851–1858.
29. Ojha, K., Pradhan, N. C. and Samanta, A. N., From ash to cash. *Bull. Mater. Sci.*, 2004, **27**, 555–564.
30. Bhasin, S., Amritphale, S. S. and Chandra, N., Effect of pyrophyllite additions on sintering characteristics of fly ash based ceramic wall tiles. *Br. Ceram. Trans.*, 2003, **102**(2), 1–4.
31. Amritphale, S. S. and Patel, M., Utilisation of red mud, fly ash for manufacturing bricks with pyrophyllite. *Silic. Indus.*, 1987, **2**(3–4), 31–35.
32. Amritphale, S. S., Chandra, N. and Bhasin, S., Optimisation of processing parameters for making pyrophyllite based ceramic tiles using di-sodium hydrogen phosphate binder. *Br. Ceram. Trans.*, 2001, **100**(6), 279–283.
33. Amritphale, S. S., Bhasin, S. and Chandra, N., Studies on sintering behaviour of pyrophyllite based ceramic tiles using di-potassium binder. *Silic. Indus.*, 2004, **69**(1–2), 14–18.
34. Amritphale, S. S., Bhasin, S. and Chandra, N., Energy efficient process for making pyrophyllite based ceramic tiles using phosphoric acid and mineralizers. *Ceram. Int.*, 2006, **32**, 181–187.
35. Kingery, W. D., Browen, H. K. and Uhlman, D. R., *Introduction to Ceramics* (*2nd ed.*). John Wiley & Sons, New York, 1976, p. 531.
36. Indian Standrad Specification No. 777 (1970) and IS-9130 (1999).
37. Vogel, l. A., *A Text Book of Quantitative Chemical Analysis* (*5th ed.*). ELBS Publication, London, U.K., 1972, p. 417.
38. Mineral Powder Diffraction File Search Manual, JCPDS. International Center for Diffraction Data, Swarthmore, USA, 1980.
39. MacKenzie, K. J. D. and Kemmitt, T., Evolution of crystalline aluminates from hybrid gel-derived precursors studied by XRD and multinuclear solid-state MAS NMR. I: Celsian $BaAl_2Si_2O_8$. *Thermochim. Acta*, 1999, **325**, 5–12.
40. Drummond, C. H. and Bansal, N. P., Crystallization behaviour and properties of $BaO{\cdot}Al_2O_3{\cdot}2SiO_2$ glass matrices. *Ceram. Eng. Proc.*, 1990, **11**(7–8), 1072–1086.
41. Boskovic, S., Kosanovic, D., Bahloul-Hourlier, Dj., Thomos, P. and Kiss, S. J., Formation of celsian from mechanically activated $BaCO_3$–Al_2O_3–SIO_2 mixtures. *J. Alloys Compd.*, 1999, **290**(1–2), 230–235.
42. Lee, K. T. and Aswath, P. B., Enhanced production of celsian barium aluinosilicates by a three-step firing technique. *Mater. Chem. Phys.*, 2001, **71**, 47–52.
43. Allameh, S. M. and Sandhage, K. H., Synthesis of celsian ($BaAl_2Si_2O_8$) from solid Ba-Al–Al_2O_3 precursors. I: XRD and SEM/EDX analyses of phase evolution. *J. Am. Ceram. Soc.*, 1997, **80**(12), 3109–3126.
44. Shigemoto, N., Hayashi, H. and Miyaura, K., Selective formation of Na–X zeolite from coal fly ash by fusion with sodium hydroxide prior to hydrothermal reaction. *J. Mater. Sci.*, 1993, **28**, 4781.
45. Zhang, X. D., Sandhage, K. H. and Fraser, H. J., Synthesis of $BaAl_2Si_2O_8$ from solid Ba–Al–Al_2O_3–SiO_2 precursors. II: TEM analyses of phase evolution. *J. Am. Ceram. Soc.*, 1999, **81**(11), 2983–2997.
46. Allameh, S. M. and Sandhage, K. H., Synthesis of celsian ($BaAl_2Si_2O_8$) from solid Ba–Al–Al_2O_3 precursors. I: XRD and SEM/EDX analyses of phase evolution. *J. Am. Ceram. Soc.*, 1997, **80**(12), 3109–3126.
47. Archer, B. A., Fewell, T. R., Conway, B. J. and Quinn, P. W., Attenuation properties of diagnostic X-ray shielding materials. *Med. Phys.*, 1994, **21**(9), 1499–1507.